Nonlin. Processes Geophys., 20, 59–69, 2013
www.nonlin-processes-geophys.net/20/59/2013/
doi:10.5194/npg-20-59-2013

Nonlinear Processes in Geophysics

Analysis of asymmetries in propagating mode-2 waves

J. Olsthoorn, A. Baglaenko, and M. Stastna

University of Waterloo, Ontario, Canada

Correspondence to: J. Olsthoorn (jolsthoo@uwaterloo.ca)

Received: 29 September 2012 – Revised: 3 December 2012 – Accepted: 4 December 2012 – Published: 16 January 2013

Abstract. Using numerical simulations performed with a pseudo-spectral incompressible Navier–Stokes solver, we describe the asymmetries that arise in the recirculating core of mode-2 internal, solitary-like waves. The waves are generated in a manner consistent with many laboratory studies, namely via the collapse of a region of mixed fluid. Analysis of the simulations reveals that asymmetries across both the wave crest and the pycnocline centre develop in the spatial distribution of density, kinetic energy and a passive tracer transported by the mode-2 waves. The simulations are extended to three-dimensions to allow for the formation of spanwise instabilities. We find that three-dimensionalization modifies the structure and energetics of the core, but that the majority of the results obtained from two dimensional simulations remain valid. Taken together, our simulations demonstrate that the cores of solitary-like mode-2 waves are different then their counterparts for mode-1 waves and that their accurate characterization on both lab and field scales should account for the core asymmetry across the pycnocline centre.

1 Introduction

Internal solitary waves (ISWs) are a commonly observed feature of coastal waters and lakes during the temperature stratified season (Helfrich and Melville, 2006; Boehrer and Schultze, 2008). These waves can transport mass (Inall et al., 2001; Lamb, 1997) and induce mixing (Scotti et al., 2004) and thereby can exert a significant impact on the nutrient circulation system and ecological communities (Lennert-Cody and Franks, 1999; Stastna, 2011).

The theoretical description of linear, horizontally propagating (or vertically trapped) internal waves in a continuously stratified fluid yields an infinite number of modes in the vertical, with the exact structure of the modes determined by the background density and horizontal velocity profiles (Grimshaw, 2003; Wiegand and Chamberlain, 1987). However, nearly all of the energy is captured by the first few modes (Wiegand and Chamberlain, 1987). In fact, the exact theory of internal solitary waves considers only mode-1 waves (Turkington and Wang, 1991). Mode-1 waves are exceptional because long mode-1 waves will outpace all other mode numbers. Thus, mode-1 nonlinear waves, which are faster than linear waves, will propagate away from an initial disturbance and achieve a solitary state (in inviscid theory). The simplest mathematical expression of this fact is contained in the Korteweg deVries equation

$$B_t = -c_{\mathrm{lw}} B_x + \alpha B B_x + \beta B_{xxx}, \tag{1}$$

where the nonlinear and dispersive coefficients, α and β, respectively, can be determined from the background density and horizontal velocity profiles (Grimshaw, 2003; Helfrich and Melville, 2006). For a corresponding viewpoint on fully nonlinear periodic internal waves see Camassa et al. (2010).

Mode-2 waves, even in the long wave limit, cannot have wave speeds that are faster than a finite length mode-1 wave. Thus, whenever mode-2 waves are observed, they are accompanied by a tail of mode-1 waves. In terms of linear wave theory, the phase speed of the mode-1 tail matches the propagation speed of the mode-2 leading wave. However, the mode-1 group velocity is smaller than the phase velocity and thus energy is slowly drained from the mode-2 wave. For this reason mode-2 waves are often referred to as solitary-like as they will slowly decay. This scenario has been formally justified using asymptotics beyond all orders in Akylas and Grimshaw (1992). These, long-lived mode-2 waves have been observed in experiments, numerical simulations and in the field (Munroe et al., 2009; Ramp et al., 2012; Shroyer et al., 2010; Vlasenko and Hutter, 2001; Dunphy et al., 2011; Sveen et al., 2002).

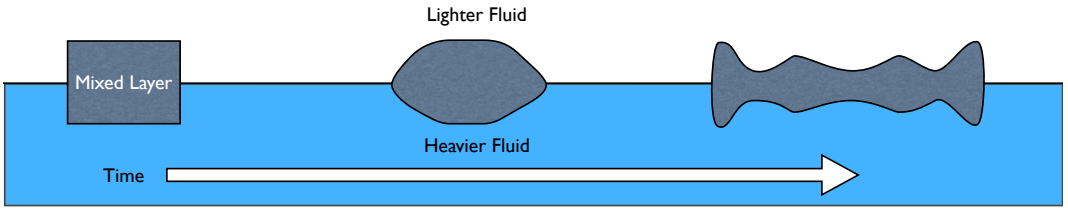

Fig. 1. Diagram of the basic experimental setup for numerical simulation.

More generally, mode-2 waves have been studied experimentally (Munroe et al., 2009; Shroyer et al., 2010; Stamp and Jacka, 1995; Vlasenko and Hutter, 2001; Yang et al., 2010), analytically (Davis and Acrivos, 1967; Stamp and Jacka, 1995) and numerically (Hodges et al., 2000; Rubino et al., 2001; Terez and Knio, 1998; Salloum et al., 2012; Dunphy et al., 2011). The typical lifecycle of mode-2 wave generation and evolution due to the collapse of an intermediate density region that is thicker (in the vertical direction) than the pycnocline is schematized in Fig. 1. Terez and Knio (1998) and Salloum et al. (2012) demonstrated that breaking mode-2 waves efficiently trap and transport particles, though a careful reading of their paper reveals that they, in fact, simulated mode-1 waves, and interpreted the results for mode-2 waves by reflecting across a line of symmetry. Indeed, nearly all theoretical discussion of mode-2 waves is provided for waves traveling along a pycnocline centred at the mid-depth of the domain. In this special case, mode-2 waves are symmetric about their centre-line (Davis and Acrivos, 1967; Stamp and Jacka, 1995). However, such a stratification is never observed in natural waters.

Several papers also suggest that first-order KdV theory yields good predictions for mode-2 propagation speeds, and reasonable predictions for wave structure (Stamp and Jacka, 1995; Terez and Knio, 1998; Vlasenko and Hutter, 2001). This is in contrast to the well-known disparity between exact mode-1 waves and those predicted by equations in the KdV hierarchy (Lamb and Yan, 1996; Lamb, 1999). For a stratification dominated by a single pycnocline, mode-2 waves overturn for moderate amplitudes. To see this consider a stratification at the mid-depth for which mode-2 waves are equivalent to mode-1 waves in a domain with a total depth of $H/2$ and a stratification with a maximum buoyancy frequency at the bottom. In the absence of a background current, such waves are well-known to yield overturning and recirculating cores (Lamb and Wilkie, 2004 and the references therein). It is thus quite possible that KdV theory yields a good prediction for both the propagation speed and the wave structure over the majority of the water column while the overturning, or core, region of the flow is fully three-dimensional.

In this paper we use numerical simulations to discuss the effects of a stratification that is not symmetric about the mid-depth. In particular, we reexamine some of the conclusions reached in Terez and Knio (1998) regarding the structure of the wave core. We demonstrate that physical mode-2 waves can become significantly asymmetric, especially in the core region, and that they develop a mode-1 wave tail.

This paper is organized as follows: we begin with a brief introduction to the theory of ISWs. We then describe the numerical model used to simulate the mode-2 waves. We demonstrate the effect of the asymmetry about the centre of the pycnocline, and demonstrate how these results generalize from two-dimensions to three-dimensions. We conclude with a discussion of the results and some suggestions for future research.

2 Theory and methods

2.1 Theory

We consider a non-rotating, incompressible fluid that obeys the Boussinesq approximation with a rigid lid. The governing Navier–Stokes equations read

$$\frac{\partial \boldsymbol{u}}{\partial t} + \boldsymbol{u}\cdot\nabla\boldsymbol{u} = -\frac{1}{\rho_0}\nabla P + \nu\nabla^2\boldsymbol{u} - \frac{\rho g}{\rho_0}\hat{k}, \tag{2}$$

$$\nabla\cdot\boldsymbol{u} = 0, \tag{3}$$

$$\frac{\partial \rho}{\partial t} + \boldsymbol{u}\cdot\nabla\rho = \kappa\nabla^2\rho, \tag{4}$$

for the velocity field **u** and pressure P, where ρ_0 is some reference density of the fluid, and $\{\nu, \kappa, g\}$ are the dynamic viscosity, the molecular diffusivity, and the acceleration due to gravity, respectively. We take the x-axis to run along the top of our domain, the z-axis to point upward, and the y-axis to represent the spanwise direction that is absent in 2-D simulations.

The theory of ISWs is based on the inviscid Euler equations which can be derived from the above by setting $\nu = \kappa = 0$. In two dimensions, incompressibility implies the existence of a stream function ψ so that $(u, w) = (\psi_z, -\psi_x)$ where subscripts denote partial derivatives. The first-order weakly nonlinear theoretical description in the absence of a background current (Grimshaw, 2003) thus assumes

$$\psi = B^{(n)}(x,t)\phi^{(n)}(z), \tag{5}$$

where n denotes the mode number. The vertical structure is determined by solving the Sturm–Liouville eigenvalue problem

$$\frac{\mathrm{d}^2\phi^{(n)}}{\mathrm{d}z^2} + \frac{N^2(z)}{c^2}\phi^{(n)} = 0 \tag{6}$$

while N^2 is the buoyancy frequency and c is the wave propagation speed. Here, the evolution of the waveform is given by the KdV equation

$$B_t^{(n)} = -c^{(n)} B_x^{(n)} + \alpha^{(n)} B^{(n)} B_x^{(n)} + \beta^{(n)} B_{xxx}^{(n)}, \tag{7}$$

where the nonlinear and dispersive coefficients, α and β, respectively, can be determined from the background density and horizontal velocity profiles (Grimshaw, 2003; Helfrich and Melville, 2006) for each mode.

For finite length linear waves with wavenumber k we have

$$\psi_{\mathrm{lin}} = a^{(n)} \exp(ikx)\phi_{\mathrm{lin}}^{(n)}(z) \tag{8}$$

where

$$\frac{\mathrm{d}^2\phi_{\mathrm{lin}}^{(n)}}{\mathrm{d}z^2} + \left(\frac{N^2(z)}{c_{\mathrm{lin}}^2} - k^2\right)\phi_{\mathrm{lin}}^{(n)} = 0. \tag{9}$$

It is thus clear that the KdV theory is a long wave ($k \to 0$) theory. The vertical structure of short waves will be oscillatory in the pycnocline, but exponential decaying in the weakly stratified regions. This has important implications when solitary-like waves coexist with shorter finite length waves since the former will induce velocities throughout the water column, while the latter will only influence the region near the pycnocline.

We model a single pycnocline density profile using a hyperbolic tangent function, thereby implying that

$$N^2(z) = a\ \mathrm{sech}^2((z - z_0)/d), \tag{10}$$

where z_0 sets the centre of the pycnocline and d sets its thickness. For the simulations reported on below, $a = 0.01$, corresponding to a 2 % top-to-bottom density change; while $d = 0.05H$ or 5 % of the total depth and z_0 varies from the purely symmetric case for which z_0 is located at the mid-depth with departures given in terms of a percentage of the total depth (5 %, 20 %, etc.).

If the profile of $N^2(z)$ is symmetric about the mid-depth, the mode-2 vertical structure function is then anti-symmetric about the mid-depth. In this situation, mode-1 ISWs cannot form producing true solitary mode-2 waves (Stamp and Jacka, 1995). Moreover, even moderate deviations of the pycnocline centre (z_0) from the mid-depth do not yield significant departures of the zero of the mode-2 structure function from the pycnocline centre. This is demonstrated in Fig. 2 which shows shaded contours of the absolute difference between the location of the zero of the mode-2 structure function and the pycnocline centre. The pycnocline centre, width, and the absolute difference are scaled by the total depth. The figure thus indicates that, as far as the linear theory is concerned, mode-2 waves can be expected to be nearly symmetric about the pycnocline centre. Since this figure shows dimensionless results, this is true for both the experimental scale and the field scale, and indeed, as has been mentioned above, this has been the standard assumption in much of the literature. It is the central point of our numerical simulations to demonstrate that this is not the case for actual finite amplitude waves.

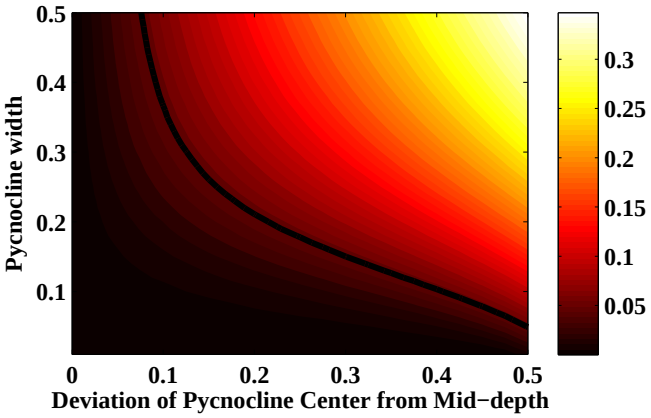

Fig. 2. Contours plot indicating the location of mode 2 wave zeros based on pycnocline centre and width. Note that as the pycnocline is moved away from the centre and thickened, the zero of the mode 2 wave function moves away from the centre of the pycnocline.

2.2 Numerical model

The numerical simulations are performed using a scalable, pseudo-spectral code (Subich, 2011), parallelized using the Message Passing Interface (MPI). MPI is a communications protocol used to parallelize the execution of an application across multiple CPUs. The code solves the full three-dimensional Navier–Stokes equations for a stratified fluid under the Boussinesq approximation (Kundu and Cohen, 2010). A standard splitting methodology is used, in which an advective step is followed by an elliptic solve for the pressure, and finally a Stokes problem imposes the no slip boundary conditions. The code does allow for variable bottom topography, as well as sidewalls; however, the configuration used herein consists of a channel with flat, no slip walls at the top and bottom and free slip side walls. Upon Fourier transforming, and employing appropriate symmetries in the streamwise and spanwise directions, the implicit equations for pressure and viscosity separate into a number of one-dimensional (in z) problems. These are iteratively solved, at each step of the simulation, using GMRES (Saad, 2003) with a finite-difference preconditioner (Boyd, 2001).

The 2-D simulations reported on use 2048×192 grid points, with grid halving studies indicating that this resolution (along with spectral accuracy) was more than adequate

(Boyd, 2001). The domain employed was 6 m in length and 0.4 m in depth. The simulations were run for 100 s, and output was saved every 2.5 s. By the end of the simulation the mode-2 waves approach the edge of the domain. The numerical situation is thus a reasonable representation of a laboratory scale setup. In the simulation we set viscosity of water to $\nu = 1 \times 10^{-6}\,\mathrm{m^2\,s^{-1}}$, with a diffusivity of $\kappa = 5 \times 10^{-7}\,\mathrm{m^2\,s^{-1}}$.

In order to evaluate the extent to which 2-D simulations faithfully represent asymmetries that would form in an actual experiment, we performed three-dimensional simulations of two of the 2-D cases. Extracting the flow profile at $t = 25$ s, we extend the various fields (density, velocity components, etc.) into the third dimension and allow the flow profile to evolve to $t = 37.5$ s. As spectral methods preserve symmetry, we introduce low-level noise to the velocity field in order to trigger any instabilities spanwise. The perturbation was defined to be white noise with a maximum of 2 % of the maximum horizontal velocity. The domain was modified to be $3 \times 0.2 \times 0.4$ m with a grid resolution of $832 \times 192 \times 96$. The reduction in domain length was reasonable, as we do not let the simulation extend past $t = 37.5$ s, where the initial mode-2 wave nearly reaches the edge of the new domain. Values of diffusivity and viscosity were the same as in the 2-D simulations. Outputs were taken twice as often as the 2-D case (1.25 s).

In order to visualize how the internal waves transport fluid, we initialize a passive tracer which is simply advected along with the flow (same diffusivity as the density). This is equivalent to the particle tracking method found in Terez and Knio (1998).

2.3 Experimental setup

Experimental realizations of mode-2 waves, as well as numerical simulations designed to mimic them such as Terez and Knio (1998), both employ a "lump" of intermediate density fluid that collapses to form the mode-2 waves. In numerical calculations the interface between the perturbing fluid and the undisturbed pycnocline is typically smoothed. For the simulations reported on below, the initial condition is chosen to be symmetric across the pycnocline centre and its mathematical form is given by

$$\rho = \bar{\rho}(z) + \rho_M(x,z) \tag{11}$$

$$\bar{\rho} = 1 - 0.01 \tanh\left(\frac{z+z_0}{0.05Lz}\right) \tag{12}$$

$$\rho_M = \frac{1}{2}\left[\sum_{i=1}^{2} \tanh\left(\frac{x+x_i}{\lambda}\right) + \sum_{j=1}^{2} \tanh\left(\frac{z+z_j}{\zeta}\right)\right] \tag{13}$$

$$(x_1, x_2) = L_x(0.9, 1.1) \tag{14}$$

$$(z_1, z_2) = L_z(z_0 - 0.15, z_0 + 0.15). \tag{15}$$

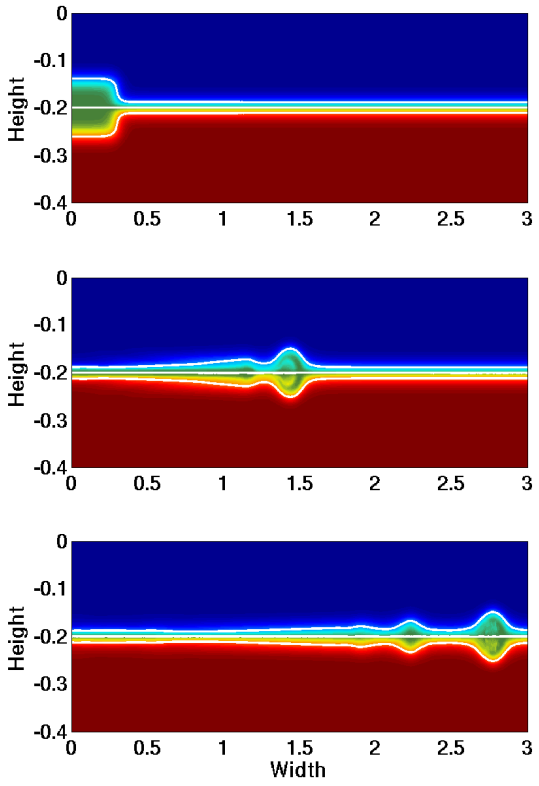

Fig. 3. Plot of the density evolution at times $t = \{0, 25, 50\}$ s. Three isocontours of density highlight the location of the mode-2 waves.

For the symmetric stratification $z_0 = L_z/2$ and for the asymmetric stratifications $z_0 = 1.1 \times L_z/2$ and $z_0 = 1.4 \times L_z/2$. We pick $\lambda = 0.05L_x$, and $\zeta = 0.02L_z$.

While this equation appears complex, Fig. 3 plots this initialization of the density field and its time evolution. Note that this figure demonstrates that the density evolution corresponds well with the cartoon of mode-2 wave generation and evolution shown in Fig. 1. To investigate the onset of asymmetry in the mode-2 waves, especially in the region of overturns, we gradually moved the centre of the pycnocline from the mid-depth. In the Sect. 3 below, three cases are discussed in detail (symmetric, 5 % and 20 % asymmetry). Since the region of overturning will lead to vortex stretching and three-dimensional flow, three-dimensional simulations are performed to investigate the physical characteristics of the flow in this region.

3 Results

3.1 Symmetric stratification

As our base case, we consider a pycnocline centred at the mid-depth of the tank. Initializing with an intermediate density layer as described above, we allow gravity to cause the mixed region to collapse, allowing mode-2 waves to be

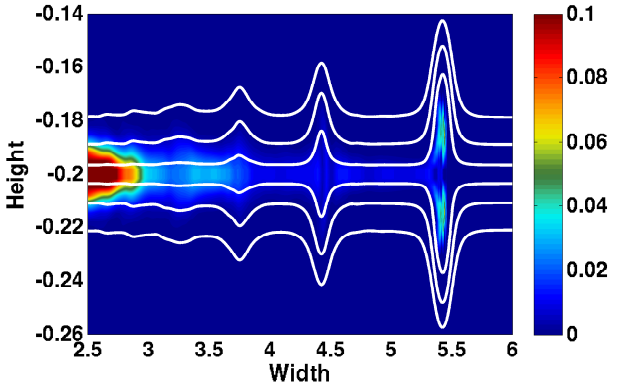

Fig. 4. Plot of the tracer concentration at $t = 100$ s for a initial mixed layer symmetric about a mid-depth pycnocline. The colorbar was saturated at 10 % of the maximum. Six contours of density are overlayed in order to identify the location of the internal waves. Notice that the distribution is entirely symmetric about the mid-depth. Three perfectly symmetric mode-2 waves are clearly observed.

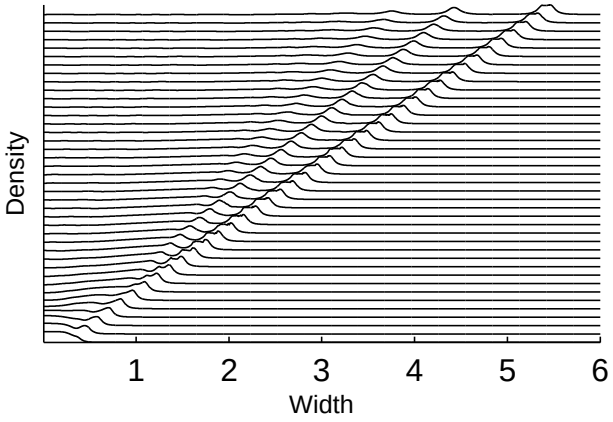

Fig. 5. Waterfall plot of the horizontal wave structure. Notice three clearly defined mode-two waves propagating in time.

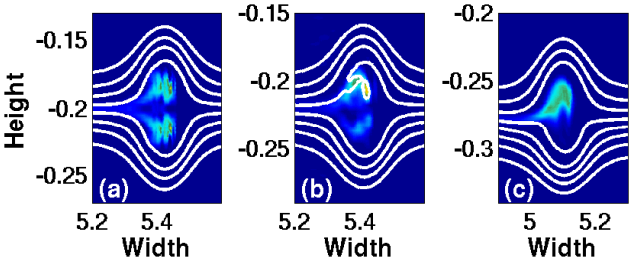

Fig. 6. A comparison of the largest mode-2 wave at time $t = 100$ s for a pycnocline centred at **(a)** $-z_0 = H/2$, **(b)** $-z_0 = H/2 + 0.05H$, and **(c)** $-z_0 = H/2 + 0.20H$. Eight isocontours of density are overlayed to depict the location of the mode-two wave. It is very clear the off-centre location of the pycnocline causes the tracer to lose its symmetry about the centre of the mode-2 wave. Colorbar is saturated to 10 % of its maximum value.

generated. As the distribution is entirely symmetric about the centre of the domain, we find no mode-1 wave formation with the mode-2 waves maintaining a perfect symmetry about the pycnocline, as the theory predicts.

Figure 4 shows the results of this simulation after 100 s. Three perfectly symmetric mode-2 waves are clearly visible with a number of smaller mode-2 waves following behind. A certain amount of tracer is trapped by the mode-2 waves as they propagate, though the majority remains behind near the location of intermediate density fluid perturbation.

Once a particular mode-2 wave forms, it will propagate along at a speed proportional to its amplitude. When the experiment is run, assuming perfect vertical symmetry, no mode-1 waves can form and thus there is no means for draining energy from the main wave, apart from effects of the viscous boundary layer (which were found to be inconsequential). Figure 5 shows a waterfall of the horizontal wave structure of the flow, constructed from density isocontours taken 5 % above the centre of the pycnocline. Here the mode-2 waves are clearly visible, as is the fact that the wave speeds are essentially constant. As expected, the largest mode-2 wave propagates faster than the smaller trailing mode-2 waves.

3.2 Off-centre pycnocline

In the simulations with a pycnocline centre that is offset from the mid-depth by 5 % and 20 % of the total depth, the essential aspects of the wave generation process remain unchanged. However, once the waves have formed, the accompanying mode-1 tail quickly becomes apparent.

Figure 6 plots the tracer found within the trapped core of the leading mode-2 wave along with eight isocontours of density at $t = 100$ s. The colorbar for this figure is saturated to 10 % of the initial tracer maximum. Notice that in the symmetric stratification case (a), we find a perfect symmetry in both the mode-2 wave and the trapped tracer within the wave core. When the pycnocline is displaced 5 % from the mid-depth (b), we find that there is already some significant differences in both tracer distribution and density profile. Note the region of overturning density contours near $(x, z) = (5.35, -0.2)$ m, or the edge of the nearly trapped core of the wave. When the pycnocline is displaced 20 % from the mid-depth (c), the tracer is almost entirely located within the upper half of the mode-2 wave with a density profile whose structure is visibly asymmetric about the pycnocline centre. Based on this figure it is clear that the picture of the trapped core, and particle transport by this core, as advanced in Terez and Knio (1998), is not representative of reality for pycnocline centres that are offset from the mid-depth by more than a few percent of the total depth.

Figure 7 shows the distribution of tracer along with seven isocontours of density in the tail of the mode-2 wave train at $t = 100$ s. The colorbar is saturated at 5 % of the initial maximum value of the tracer. Notice that the symmetric

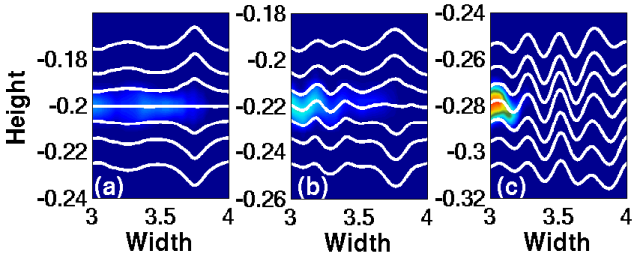

Fig. 7. A comparison of the tail behind the two largest mode-2 waves at time $t = 100$ s for a pycnocline centred at **(a)** $-z_0 = H/2$, **(b)** $-z_0 = H/2 + 0.05H$, and **(c)** $-z_0 = H/2 + 0.20H$. Seven isocontours of density are overlayed to depict the location of the mode-1 waves. Notice that there are no mode-1 waves when the pycnocline is at the mid-depth. As the pycnocline is displaced from centre, mode-1 waves quickly develop, eventually dominating the tail.

stratification case (a) has no mode-1 waves behind the last coherent mode-2 wave. When the pycnocline centre is displaced 5 % (b) from the mid-depth, we find that some small mode-1 waves develop in the tail while the mode-2 wave is still clearly visible at the front. However, once the pycnocline is displaced 20 % (c) from the centre of the domain, the mode-1 waves almost completely dominate any mode-2 waves present. Upon close inspection, one can see that the front of this tail is a superposition of a mode-1 and mode-2 wave. A second point to note is that as the pycnocline is displaced from centre, the tracer is not transported as far from the initial perturbation.

In all simulations, after an initial period of adjustment, the estimated wave speed of the leading waves appear to be nearly constant up to the end of the simulations (100 s). We compared the computed wave speeds of the leading mode-2 waves with the KdV prediction and found that the error of the simulated wave speeds was less than 1 % for the symmetric and 5 % cases. The small decrease can be attributed to viscous effects. Since viscosity only plays an important role near the solid top and bottom boundaries, the decrease in wave speed for these cases was small. When the pycnocline is significantly displaced from the mid-depth, one of the two near boundary regions will have stronger wave-induced currents, and the effect on the wave speed can be expected to be larger. In particular, for the 20 % shift, the estimated wavespeed was decreased by less than 4 %. It is unclear whether this is primarily due to viscous effects or the change in wave shape from the idealized KdV soliton due to the presence of a recirculating core. For large shifts (e.g. 40 %) the interaction with the boundary layer can be expected to become dominant, and this provides a direction for future study.

3.3 Asymmetry

A quantitative measure of the asymmetry of the core can be derived by integrating the total amount of tracer above and below the pycnocline centre and subtracting these two values for each value of x. Figure 8 shows a waterfall plot of this asymmetry measure when the pycnocline is displaced by 5 % (a) and 20 % (b). As before, density profiles taken 5 % above the pycnocline are plotted at every time step. In panel (c) of this figure, the maximum of the asymmetry measure is plotted as a function of time. We note that the maximum asymmetry is observed to correspond to the path of the largest mode-2 wave. This is consistent with the distribution of tracer shown in Fig. 6. Since the core is not perfectly trapping, the asymmetry decays over time as material is left behind by the wave. In the long run, the tracer tends to a symmetric distribution about the pycnocline, though this is the trivial state of no tracer left in the wave.

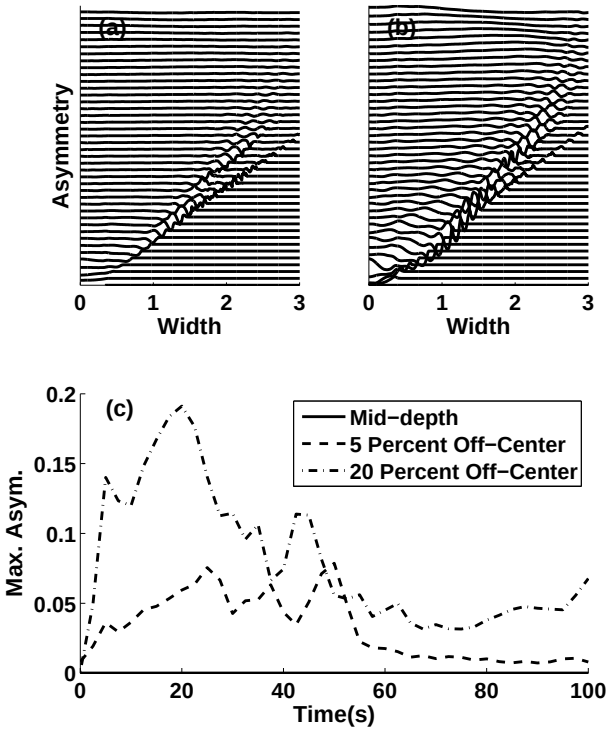

Fig. 8. Waterfall plot of the asymmetry in the tracer about the pycnocline for **(a)** $-z_0 = H/2 + 0.05H$, and **(b)** $-z_0 = H/2 + 0.20H$. **(c)** Plot of the maximum asymmetry versus time.

We know that the above discussed asymmetry is associated with the formation of a mode-1 tail, which will slowly drain energy from the mode-2 waves. To quantify the amount of energy drained into the mode-1 tail, Fig. 9 shows shaded contours of the kinetic energy of the flow at $t = 100$ s. Here the colorbar is saturated to 10 % of the maximum kinetic energy in the fluid. Four isocontours of density were also plotted in order to highlight the location of the various mode-2 waves and the mode-1 tail. The kinetic energy plot very clearly highlights the dominance of the mode-2 waves. While the kinetic energy induced by the mode-1 tail is not negligible, we have determined that the maximum kinetic energy in the tail is only 5.68 % of the maximum kinetic energy of the

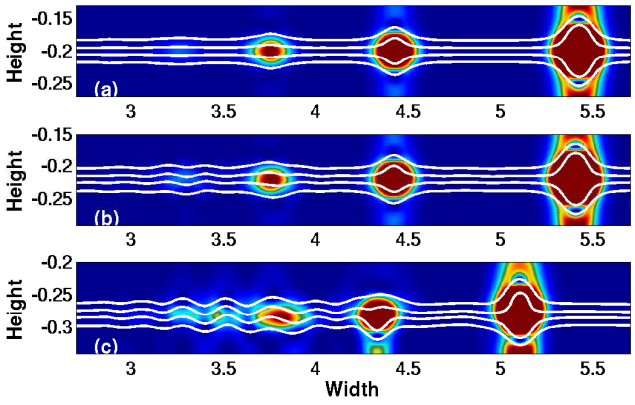

Fig. 9. Plot of the kinetic energy at $t = 100$ s for the symmetric **(a)**, 5 % **(b)** and 20 % **(c)** shifts. The colorbar was saturated at 10 % of the maximum value of the symmetric case.

flow. Thus, while the mode-1 tail does influence the evolution of the leading mode-2 waves, it will do so on long time scales, and the asymmetry induced by the breaking of the mode-2 waves will dominate in an experimental, and likely in a field, setting.

In the 20 % shift case it can been that there is some evidence of wave-induced kinetic energy beneath, but not above, the pycnocline for the second mode-2 wave. This is due to the conservation of volume which necessarily amplifies the horizontal velocity in the narrower layer (found below the pycnocline in this case). This occurs for all the waves, but is visually the most apparent for the second mode-2 wave. At the saturation level chosen, the leading wave induces significant currents throughout the portion of the domain shown. However, a careful examination of the region near $x = 5.1$ shows the same pattern of amplification as for the second wave.

Finally, we note that numerical experiments in which the initially mixed region is centred about the height of the zero of the mode-2 wave structure function, with a density of the mixed region chosen to match that the of the upstream density profile at the height of the zero of the mode-2 wave structure function, yielded nearly identical results as far as the asymmetry of the wave core. The significant asymmetry is thus a generic feature of breaking mode-2 waves generated by the collapse of a mixed region.

3.4 Three-dimensional effects

While the two dimensional results are representative of the early stages of wave evolution, three-dimensional effects will come into play as the overturns in the core region undergo spanwise instabilities. We extend the flow profile at $t = 25$ s into the third dimension, as described in the Methods Sect. 2.2, and follow its evolution. Figure 10 shows the evolution of the streamwise average of the spanwise standard deviation of kinetic energy as a function of distance from pycnoline at $t = \{33.75\,\text{s (a)}, 35\,\text{s (b)}, 36.25\,\text{(c)}, 37.5\,\text{s (d)}\}$. All panels were normalized to the maximum value of the symmetric case at $t = 37.5$ s. We find that the spanwise variation takes longer to develop for the 20 % shift than it does for the symmetric case. This is due to the faster wave speeds found within the symmetric case. That is, the maximum average variation is higher for the symmetric case earlier in the three-dimensionalization while the variation ramps up for the off-centre case. However, as is clearly demonstrated in Fig. 10, the mean spanwise variation nearly quadruples over the 3.75 s before $t = 37.5$ s. We see then that the most significant spanwise variation occurs at the end of the above simulation. Here the 20 % shift case had a maximum average spanwise variation that was 12 % greater than the corresponding symmetric case.

To get an idea of which portions of the wave are associated with three-dimensional motions, we plot the spanwise standard deviation of the density and kinetic energy fields at $t = 37.5$ s, at which time both cases have achieved significant three-dimensionalization. The maximum spanwise variation at this point is about 10–20 % of the maximum kinetic energy. In Fig. 11, panels (a) and (b) contrast the standard deviation of the density field for the symmetric and 20 % cases. It can be seen that the symmetric stratification maintains a great deal of symmetry across the mid-depth even as the fluid motions three-dimensionalize in and around the core of the leading mode-2 wave. This is consistent with panels (c) and (d) which show the standard deviation of the kinetic energy. Physical dimensions have been scaled out by $d = 1$ m. We note that while the three-dimensionalization is constrained to within the core region of the initial mode-2 wave, the spatial structure of the variation is strikingly different. The symmetric case maintains a variation that is symmetric about the pycnocline, with a spatial structure located essentially in the centre of the mode-2 wave. This is in contrast to the asymmetric 20 % pycnocline shift case, where the variation is positioned towards the back of the core region with most of the variation occurring near the edge of the core. The panels have been scaled by the background density jump across the pycnocline and the maximum value of kinetic energy standard deviation for the symmetric case. The maximal spanwise density variation is equal to 1.67 % of the background density jump across the pycnocline in the symmetric case, but this increases to 3.09 % for the 20 % shift.

The spanwise structure of the three-dimensionalization is shown in Fig. 12 for the symmetric stratification case at $t = 37.5$ s. Dimensions are presented in dimensionless form with scaling $d = 1$ m. The figure shows two opaque density surfaces above (green) and below (yellow) as well as the regions where v^2 equals 5 % of its maximum value. It can be seen that all of the active three-dimensionalization occurs in the core region. At the back of the plot an $x - z$ slice of the horizontal velocity is shown. Here the variation is symmetric across the pycnocline.

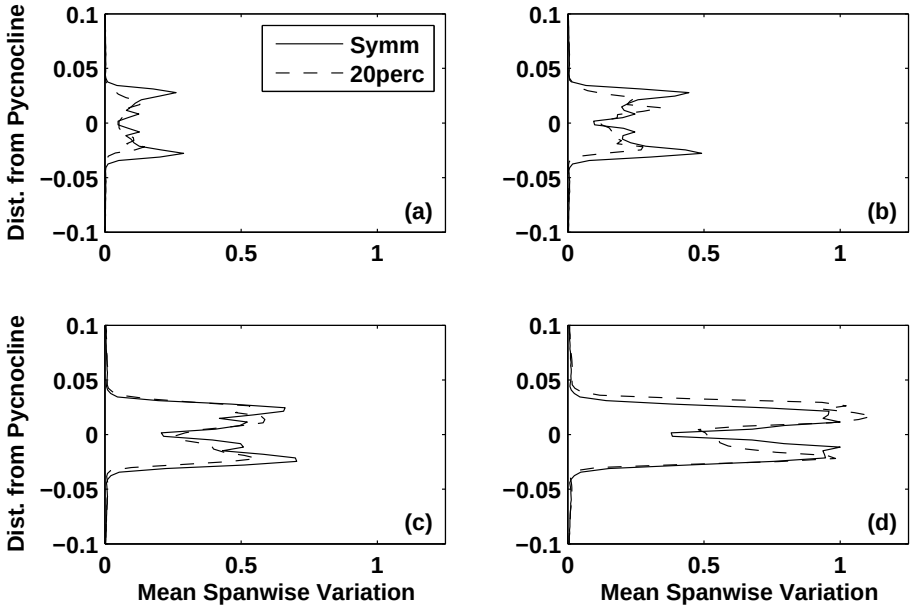

Fig. 10. Plot of the streamwise average of the standard deviation in the spanwise direction of the kinetic energy at $t = \{33.75\,\text{s}$ **(a)**, $35\,\text{s}$ **(b)**, 36.25 **(c)**, $37.5\,\text{s}$ **(d)**$\}$. The z-axis has been shifted for the asymmetric case so that both pycnocline centres are at 0. The fields were normalized by the maximum value of the symmetric case at $t = 37.5\,\text{s}$.

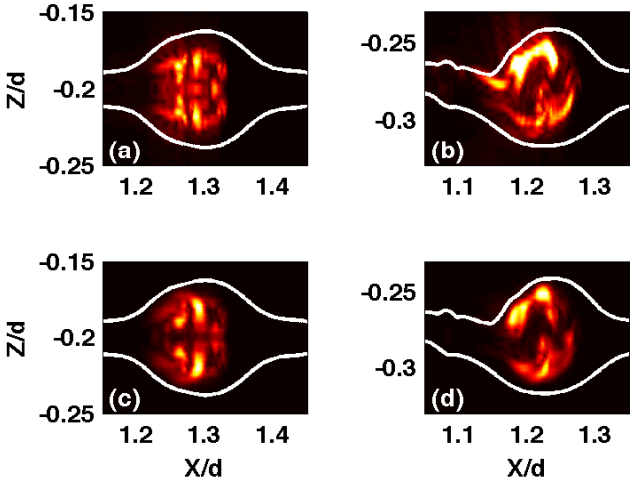

Fig. 11. A plot of the spanwise standard deviation in the density field for the symmetric **(a)** and 20 % **(b)** cases and the spanwise standard deviation in kinetic energy for the symmetric **(c)** and 20 % **(d)** cases. The region shown was cropped to show the core region of the leading wave. Image output at $t = 37.5\,\text{s}$. Two contours of density were plotted in order to highlight the location of the mode-2 wave. Images have been scaled by the background density jump across the pycnocline and the maximum value of the standard deviation of kinetic energy for the symmetric case. Scaling $d = 1\,\text{m}$.

We define a metric of the amount of spanwise flow as follows:

$$R_{\text{3-D}} = \frac{v^2}{\left(u^2 + v^2 + w^2\right)}. \tag{16}$$

For this symmetric case, we find that $R_{\text{3-D}} = 1.764 \times 10^{-2}$.

We similarly plot the effect of three-dimensionalization for the 20 % asymmetric pycnocline case in Fig. 13. As before, $d = 1\,\text{m}$. We find that the spanwise velocity is similarly localized to within the core of the initial mode-2 wave. However, the spanwise flow is located primarily above the pycnocline, where the majority of the overturning was observed in the 2-D case. Here $R_{\text{3-D}} = 3.065 \times 10^{-2}$, or approximately double the symmetric case. As with Fig. 11, we note that the majority of the three-dimensionalization occurs at the edge of the core region.

4 Discussion and conclusion

We have presented numerical simulations of the generation and propagation of mode-2 waves formed by the collapse of a mixed region of fluid. A single pycnocline stratification was chosen and hence the mode-2 waves generated were found to exhibit a recirculating core of mixed fluid, even for moderate wave amplitudes. We have found that even a moderate displacement of the pycnocline centre from the mid-depth leads to significant asymmetry in the wave core across the pycnocline centre. This asymmetry develops in both the density and kinetic energy fields as well as in the distribution of

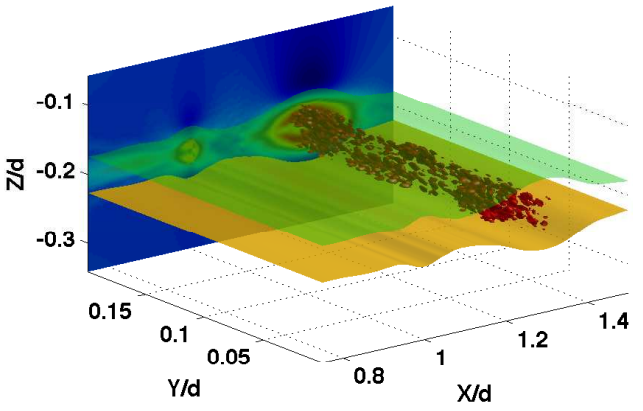

Fig. 12. Three-dimensional plot of the five percent isosurface of the maximum spanwise velocity for the symmetric case. Two isosurfaces of density were also plotted at 25 percent above (yellow) and below (green) the average density. Finally, the average horizontal velocity is also displayed on the back plane of the image, normalized to its maximum value. Image output at $t = 37.5$ s. Scaling $d = 1$ m.

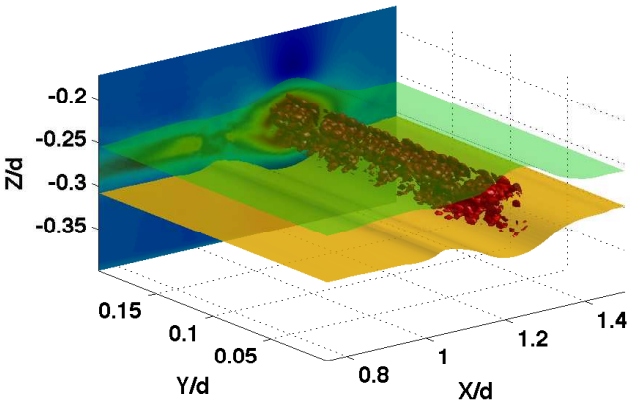

Fig. 13. Similar layout to Fig. 12 for the 20 % case. Note the significant amount of spanwise flow traveling with the core of the initial mode-2 wave. Image output at $t = 37.5$ s. Isosurfaces of the spanwise velocity field were taken at 5 % of its maximum value. Scaling $d = 1$ m.

a passive tracer that is initially symmetric across the pycnocline centre. This result is in contrast to published results (Terez and Knio, 1998; Salloum et al., 2012) and we have provided an explanation for this discrepancy. Namely, Terez and Knio (1998); Salloum et al. (2012) simulated mode-1 waves with recirculating cores, and reflected their results about the presumed centre of the pycnocline. Indeed, when the centre of the pycnocline is located precisely at the mid-depth, our results agree with Terez and Knio (1998); Salloum et al. (2012).

The recent paper by Salloum et al. (2012) builds on the past results of Terez and Knio (1998), with the same restriction to perfectly symmetric pycnoclines. In their paper, the authors discuss mass transport by large mode-2 waves and make note that instabilities within the wave core result in less mass transported by the mode-2 wave. Our current work suggests that the asymmetries developed within the mode-2 wave have the potential to amplify existing instabilities and even induce new types of instability within the core. Thus, we suggest that the mass transported by physical mode-2 waves could be significantly less than that predicted based on models with a perfectly symmetric pycnocline. This should be addressed by three-dimensional simulations and laboratory work in the future. Indeed, three-dimensional equivalents of the simulations of Terez and Knio (1998); Salloum et al. (2012) could be compared to the experiments of Grue et al. (2000) on mode-1 breaking waves.

Since it is generally accepted that weakly nonlinear theory provides a good estimate of the mode-2 wave propagation speed, and a reasonable estimate of the wave structure outside of the recirculating core, it is the dynamics of the core region that is the most appropriate focus for numerical simulations. By performing three-dimensional simulations we were able to characterize the manner in which the core three-dimensionalizes. We found that when the pycnocline centre is exactly at the mid-depth, three-dimensionalization does lead to a small amount of asymmetry across the pycnocline centre. When the pycnocline centre is displaced by 20 % from the mid-depth, the process of three-dimensionalization itself is asymmetric across the pycnocline centre, and the strength of three-dimensional motions is increased over the symmetric case.

Taken together, these results have a number of implications. In a laboratory setting, these results suggest that for the core to reach a quasi-static regime, and thus to answer whether mode-2 cores reach a quasi-steady state as has been suggested for mode-1 waves (Derzho and Grimshaw, 1997), a very long tank is necessary. However, to explore the three-dimensionalization of these cores following the collapse of the mixed region, a narrow tank of a reasonable length would prove sufficient. Moreover, the most relevant experimental work will be generated when the stratification centre is displaced form the mid-depth.

Implications of the present results to field work are a bit more speculative. Since the dominant effect of a recirculating core is the potential for long-distance transport, the asymmetry of the tracer distribution (shown in Fig. 6) suggests that any tracer transported a long distance by a mode-2 wave with a recirculating core would be found above (below) the pycnocline centre when the pycnocline centre is below (above) the mid-depth. The presence of a strong background shear current could modify this prediction, though a strong current would likely affect the structure of the mode-2 waves themselves long before a recirculating core formed. In the field, mode-2 waves do not exist in isolation and a secondary effect of the asymmetry observed, and quantified, in our simulations would be in the interaction of mode-2 waves with longer mode-1 waves. This is due to the fact that mode-1

waves induce horizontal currents of opposite polarity across the pycnocline. Returning again to Fig. 6, a mode-1 wave of elevation overtaking the mode-2 wave shown would induce currents against the direction of propagation above the pycnocline centre, and this could flush some of the trapped tracer out of the mode-2 core. In a similar manner, a head-on interaction with a mode-1 wave could serve to enhance the trapping of tracer in the mode-2 wave's core. Simulations of this process provide a clear avenue for future work, as would an effort to scale up the present simulations to larger domains while maintaining the necessary resolution in the core region.

It is this last point that has the strongest relation to past studies of cores in mode-1 waves. Mode-1 waves have a considerably larger extent and their cores can range from nearly quiescent to highly turbulent (Carr et al., 2012; Helfrich and White, 2010; Lamb and Wilkie, 2004; Michallet and Ivey, 1999). Our simulations have the closest analogy with those of Carr et al. (2012), who considered cores with weak instabilities, though it is interesting that we found significant, if not dominant, three-dimensionalization, while all past simulations, to our best knowledge, have been two dimensional.

Appendix A

Non-dimensional results

The above physical problem can be reduced to non-dimensional form in the following manner:

$$\frac{\partial \tilde{\boldsymbol{u}}}{\partial t} + \tilde{\boldsymbol{u}} \cdot \tilde{\boldsymbol{\nabla}} \tilde{\boldsymbol{u}} = -\tilde{\boldsymbol{\nabla}} \tilde{P} + \frac{1}{Re} \tilde{\nabla}^2 \tilde{\boldsymbol{u}} - Ri \tilde{\rho} \hat{k}, \tag{A1}$$

$$\tilde{\boldsymbol{\nabla}} \cdot \tilde{\boldsymbol{u}} = 0, \tag{A2}$$

$$\frac{\partial \tilde{\rho}}{\partial t} + \tilde{\boldsymbol{u}} \cdot \tilde{\boldsymbol{\nabla}} \tilde{\rho} = \frac{1}{Re} \frac{1}{Sc} \tilde{\nabla}^2 \tilde{\rho}, \tag{A3}$$

where tildes denote non-dimensional quantities. *Re*, *Ri*, and *Sc* are the dimensionless Reynolds number, Richardson number and Schmidt number, respectively. Each of these is defined as

$$Re = \frac{UL}{\nu} \qquad Ri = \frac{gL}{U^2} \qquad Sc = \frac{\nu}{\kappa}$$

for characteristic values of velocity (U), length (L), viscosity (ν), and molecular diffusion (κ). In the present paper, looking at the velocity of the initial propagating mode-2 wave, we determine our characteristic velocity to be $U = 0.05\,\mathrm{m\,s^{-1}}$. The characteristic height, viscosity and diffusivity are given as $L = 0.1\,\mathrm{m}$, $\nu = 1\times10^{-6}\,\mathrm{m^3\,s^{-2}}$, $\kappa = 5\times10^{-7}\,\mathrm{m^3\,s^{-2}}$. The gravitational acceleration is rounded to a value of $10\,\mathrm{m\,s^{-2}}$. The corresponding dimensional quantities are then computed to give

$$Re = 5000 \qquad Ri = 400 \qquad Sc = 2.$$

Acknowledgements. This research was supported by the Natural Sciences and Engineering Research Council of Canada. Christopher Subich assisted with the set up of the numerical simulations.

Edited by: V. I. Vlasenko
Reviewed by: M. Carr and J. Grue

References

Akylas, T. R. and Grimshaw, R. H. J.: Solitary internal waves with oscillatory tails, J. Fluid Mech., 242, 279–298, 1992.

Boehrer, B. and Schultze, M.: Stratification of lakes, Rev. Geophys., 46, RG2005, doi:10.1029/2006RG000210, 2008.

Boyd, J.: Chebyshev and Fourier spectral methods: Second revised edition, Dover books on mathematics, Dover Publications, 2001.

Camassa, R., Rusås, P.-O., Saxena, A., and Tiron, R.: Fully nonlinear periodic internal waves in a two-fluid system of finite depth, J. Fluid Mech., 652, 259–298, doi:10.1017/S0022112010000054, 2010.

Carr, M., King, S. E., and Dritschel, D. G.: Instability in internal solitary waves with trapped cores, Phys. Fluids, 24, 016601, doi:10.1063/1.3673612, 2012.

Davis, R. E. and Acrivos, A.: Solitary internal waves in deep water, J. Fluid Mech., 29, 593–607, doi:10.1017/S0022112067001041, 1967.

Derzho, O. G. and Grimshaw, R.: Solitary waves with a vortex core in a shallow layer of stratified fluid, Phys. Fluids, 9, 3378–3385, doi:10.1063/1.869450, 1997.

Dunphy, M., Subich, C., and Stastna, M.: Spectral methods for internal waves: indistinguishable density profiles and double-humped solitary waves, Nonlin. Processes Geophys., 18, 351–358, doi:10.5194/npg-18-351-2011, 2011.

Grimshaw, R.: Internal solitary waves, in: Environmental Stratified Flows, vol. 3 of *Topics in Environmental Fluid Mechanics*, 1–27, Springer US, 2003.

Grue, J., Jensen, A., Rusås, P., and Sveen, J. K.: Breaking and broadening of internal solitary waves, J. Fluid Mech., 413, 181–217, 2000.

Helfrich, K. R. and Melville, W. K.: Long nonlinear internal waves, Annu. Rev. Fluid Mech., 38, 395–425, doi:10.1146/annurev.fluid.38.050304.092129, 2006.

Helfrich, K. R. and White, B. L.: A model for large-amplitude internal solitary waves with trapped cores, Nonlin. Processes Geophys., 17, 303–318, doi:10.5194/npg-17-303-2010, 2010.

Hodges, B. R., Imberger, J., Saggio, A., and Winters, K. B.: Modeling basin-scale internal waves in a stratified lake, Limnol. Oceanogr., 45, 1603–1620, 2000.

Inall, M., Shapiro, G. I., and Sherwin, T. J.: Mass transport by nonlinear internal waves on the Malin shelf, Cont. Shelf Res., 21, 1449–1472, 2001.

Kundu, P. and Cohen, I.: Fluid mechanics, Academic Press, Elsevier, 2010.

Lamb, K. G.: Particle transport by nonbreaking, solitary internal waves, J. Geophys. Res., 102, 18641–18660, 1997.

Lamb, K. G.: Theoretical descriptions of shallow-water solitary internal waves: Comparisons with fully nonlinear waves, Woods Hole Oceanographic Institution Technical Report, 1999.

Lamb, K. G. and Wilkie, K. P.: Conjugate flows for waves with trapped cores, Phys. Fluids, 16, 4685–4695,

doi:10.1063/1.1811551, 2004.

Lamb, K. G. and Yan, L.: The evolution of internal wave undular bores: Comparisons of a fully nonlinear numerical model with weakly nonlinear theory, J. Phys. Oceanogr., 26, 2712–2734, 1996.

Lennert-Cody, C. and Franks, P.: Plankton patchiness in high-frequency internal waves, Mar. Ecol.-Prog. Ser., 186, 59–66, 1999.

Michallet, H. and Ivey, G.: Experiments on mixing due to internal solitary waves breaking on uniform slopes, J. Geophys. Res., 104, 13467–13477, 1999.

Munroe, J., Voegeli, C., Sutherland, B., Birman, V., and Meiburg, H.: Intrusive gravity currents from finite-length locks in a uniformly stratified fluid, J. Fluid Mech., 615, 245–273, 2009.

Ramp, S. R., Yang, Y. J., Reeder, D. B., and Bahr, F. L.: Observations of a mode-2 nonlinear internal wave on the northern Heng-Chun ridge south of Taiwan, J. Geophys. Res.-Oceans, 117, C03043, doi:10.1029/2011JC007662, 2012.

Rubino, A., Brandt, P., and Weigle, R.: On the dynamics of the internal waves in a nonlinear, weakly non-hydrostatic three-layer ocean, J. Geophys. Res., 106, 26899–26915, 2001.

Saad, Y.: Iterative methods for sparse linear systems, Society for Industrial and Applied Mathematics, Philadelphia, 2003.

Salloum, M., Knio, O. M., and Brandt, A.: Numerical simulation of mass transport in internal solitary waves, Phys. Fluids, 24, 016602, doi:10.1063/1.3676771, 2012.

Scotti, A., Beardsley, R. C., Butman, B., and Anderson, S.: Large internal waves in Massachusetts bay. Part 1: Observations, statistical properties and energetics, Geophys. Res. Lett., 31, L22307, doi:10.1.1.158.360, 2004.

Shroyer, E., Moum, J., and Nash, J.: Mode 2 waves on the continental shelf: Ephemeral components of the nonlinear internal wavefield, J. Geophys. Res.-Oceans, 115, C07001, doi:10.1029/2009JC005605, 2010.

Stamp, A. P. and Jacka, M.: Deep-water internal solitary waves, J. Fluid Mech., 305, 347–371, doi:10.1017/S0022112095004654, 1995.

Stastna, M.: Resonant generation of internal waves by short length scale topography, Phys. Fluids, 23, 116601, doi:10.1063/1.3658773, 2011.

Subich, C.: Simulation of the Navier-Stokes equations in three dimensions with a spectral collocation method, Ph.D. thesis, University of Waterloo, 2011.

Sveen, J. K., Guo, Y., Davies, P. A., and Grue, J.: On the breaking of internal solitary waves at a ridge, J. Fluid Mech., 469, 161–188, doi:10.1017/S0022112002001556, 2002.

Terez, D. E. and Knio, O. M.: Numerical simulations of large-amplitude internal solitary waves, J. Fluid Mech., 362, 53–82, 1998.

Turkington, B. Eydeland, A., and Wang, S.: A computational method for solitary internal waves in a continuously stratified fluid, Stud. Appl. Math., 85, 93–127, 1991.

Vlasenko, V. I. and Hutter, K.: Generation of second mode solitary waves by the interaction of a first mode soliton with a sill, Nonlin. Processes Geophys., 8, 223–239, doi:10.5194/npg-8-223-2001, 2001.

Wiegand, R. C. and Chamberlain, V.: Internal waves of the second vertical mode in a stratified lake, Limnol. Oceanogr., 32, 29–42, 1987.

Yang, Y. J., Fang, Y. C., Tang, T. Y., and Ramp, S. R.: Convex and concave types of second baroclinic mode internal solitary waves, Nonlin. Processes Geophys., 17, 605–614, doi:10.5194/npg-17-605-2010, 2010.